Cauliflower fractal forms arise from perturbations of floral gene networks

Eugenio Azpeitia, Gabrielle Tichtinsky, Marie Le Masson, Antonio Serrano-Mislata, Jérémy Lucas, Veronica Gregis, Carlos Gimenez, Nathanaël Prunet, Etienne Farcot, Martin Kater, et al.

Cauliflower fractal forms arise from perturbations of floral gene networks

Eugenio Azpeitia[1,‡], Gabrielle Tichtinsky[2], Marie Le Masson[2], Antonio Serrano-Mislata[3], Jérémy Lucas[2], Veronica Gregis[4], Carlos Gimenez[3], Nathanaël Prunet[5], Etienne Farcot[6], Martin M.Kater[4], Desmond Bradley[7], Francisco Madueño[3], Christophe Godin[1,*], Francois Parcy[2,*]

1: Laboratoire de Reproduction et Développement des Plantes, Univ. Lyon, ENS de Lyon, UCB Lyon 1, CNRS, INRAE, Inria, 46 allée d'Italie, F-69364, Lyon, France
2: Laboratoire Physiologie Cellulaire et Végétale, Univ. Grenoble Alpes, CNRS, CEA, INRAE, IRIG-DBSCI-LPCV, 17 avenue des martyrs, F-38054, Grenoble, France
3: Instituto de Biología Molecular y Celular de Plantas (IBMCP), Consejo Superior de Investigaciones Científicas (CSIC) - Universidad Politécnica de Valencia (UPV), 46022 Valencia, Spain.
4: Dipartimento di Bioscienze, Università degli Studi di Milano, Via Celoria 26, 20133 Milan, Italy
5: Division of Biology and Biological Engineering, California Institute of Technology, 1200 E. California Blvd., Pasadena, CA 91125, USA and Department of Molecular, Cell and Developmental Biology, University of California, Los Angeles, 610 Charles E. Young dr. S., Los Angeles, CA 90095, USA
6: School of Mathematical Sciences, University of Nottingham, NG7 2RD, United Kingdom.
7: Department of Cell and Developmental Biology, John Innes Centre, NR4 7UH Norwich NR4 7UH, United Kingdom.
‡: Present address, Centro de Ciencias Matemáticas, Universidad Nacional Autónoma de México, Morelia, México
*: Co-corresponding authors.

One Sentence Summary

The molecular making of cauliflowers

Abstract

Throughout development, plant meristems regularly produce organs in defined spiral, opposite or whorl patterns, called phyllotaxis. Cauliflowers present an unusual phyllotaxis with a multitude of spirals nested over a wide range of scales. How such a fractal self-similar organization emerges from developmental mechanisms has remained elusive. Combining experimental analyses in *Arabidopsis thaliana* cauliflower-like mutant with modeling, we found that curd self-similarity arises because the meristems fail to form flowers but keep the "memory" of their transient passage in a floral state. Additional mutations affecting meristem growth can induce the production of conical phyllotactic structures reminiscent of the conspicuous fractal Romanesco shape. This study reveals how fractal-like forms may emerge from the combination of key, defined perturbations of floral developmental programs and growth dynamics.

Main Text

Above-ground plant architectures arise from activity of shoot apical meristems (SAM), which are pools of stem cells that give rise to organs such as leaves, shoots or flowers. The arrangement of organs on stems is termed phyllotaxis. Plants with a spiral phyllotaxis usually form two families of organ spirals, visible on compact structures such as flower heads, pine cones or cacti (Fig. 1a-c). These two families of spirals turn in opposite directions, and come in two consecutive numbers of the Fibonacci series (Fig. 1a) (*1*). In cauliflowers, spiral families are visible not only at one but at several scales (Fig. 1d-f). This self-similar organization culminates in the Romanesco cultivar where the spirals appear in relief due to their conical shape at all scales, a geometrical feature conferring the whole curd a marked fractal-like aspect (Fig. 1g).

Cauliflowers (*Brassica oleracea* var. *botrytis)* were domesticated from cabbages (*2*). The cauliflower inflorescence (the shoot bearing flowers) takes a curd shape because each emerging

flower primordia never matures to the floral stage but instead generates more curd-shaped inflorescences (*2*, *3*). In *B. oleracea*, the genetic modifications causing curd development are still debated and likely affect multiple genes (*2–5*). However, cauliflower-like structures also exist in the model brassicaceae *Arabidopsis thaliana* and are caused by a double mutation in *APETALA1* (*AP1*) and *CAULIFLOWER* (*CAL*) (Fig. 1h-i), two paralogous genes encoding MADS-box transcription factors (TF) promoting floral development (*6*, *7*). The Arabidopsis molecular regulators governing the development of shoots and flowers have been largely identified (*8–10*)(Table S1). Network models based on these regulators have been proposed to explain wild-type flower development (*11–14*). However, whether variants of these networks are able to account for development of Arabidopsis *ap1 cal* curds is unknown.

To address this question, we first built a network of the main regulators involved in both flower and curd development. Then, we embedded this network within a 3D computational model of plant development to understand how mutations could transform wild-type (WT) inflorescences into curds.

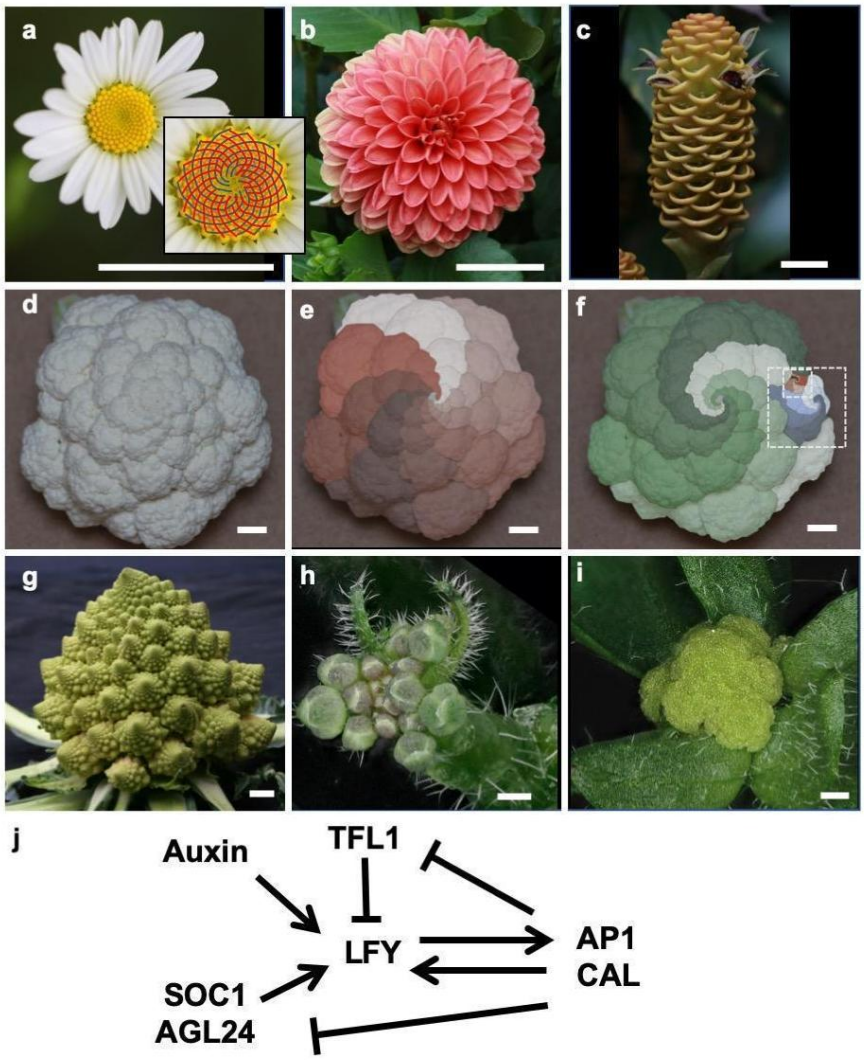

Figure 1: Illustrations of phyllotactic spirals on plant inflorescences

(a) Daisy capitulum: the two families of spirals are indicated in the close-up (13 blue spirals and 21 red). (b) Dahlia composite flower (c) Zingiber inflorescence. (d-f) *Brassica oleracea* var. *botrytis* cauliflower with (e) 8 counterclockwise (brown family) and (f) 5 clockwise (green family) main spirals. Dashed rectangles show families of spirals nested over several scales (g) Romanesco curd, (h) Arabidopsis wild-type inflorescence (h) and *ap1 cal* curd (i), Bar = 2 cm (a-g), 500 µm (h-i). (j) Interactions between major floral regulators; arrows depict activation whereas barred lines indicate repression.

The genetic basis of cauliflower curds

In Arabidopsis, flowers are initiated by the TF LEAFY (LFY) (Fig. 1j) (Table S1). *LFY* is upregulated by the SUPPRESSOR-OF-OVEREXPRESSION-OF-CO 1 (SOC1) and AGAMOUS-LIKE 24 (AGL24) MADS-box proteins (induced throughout the inflorescence meristem by environmental and endogenous cues) and by auxin phytohormone maxima that mark floral meristem initiation sites. *LFY* is expressed specifically in floral primordia because its induction in the SAM is repressed by the TFL1 inflorescence identity protein. In the floral primordium, LFY induces *AP1* and *CAL* (*AP1/CAL*) that positively feedback on *LFY* and repress both *SOC1*/*AGL24* and *TFL1*, thereby stabilizing the floral fate of the new meristem. In the *ap1 cal* cauliflower mutant, the AP1/LFY positive feedback is absent and *TFL1* is not repressed by AP1/CAL in the nascent floral meristem. Consequently, young flower primordia cannot maintain *LFY* expression and start themselves expressing *TFL1*. As a result, they lose their floral identity and become inflorescence meristems (*6*). Whereas *TFL1* repression in nascent flower primordia is well understood, the factors directly responsible for its upregulation in *ap1 cal* and inflorescence meristems are unknown.

To complete our network, we thus searched for direct positive regulators of *TFL1*, other than LFY (that induces *TFL1* (*15*) but is not active in inflorescence meristems). *TFL1* is indirectly regulated by day length (*16*): in long days (LD) *TFL1* is up-regulated by CONSTANS (CO) and FT, two key upstream effectors of the LD pathway (*11*, *17–19*) (Fig. S1). To search for direct regulators, we examined SOC1 and AGL24 that act downstream of CO and FT in the LD pathway (*9*). Loss- and gain-of-function experiments demonstrated that both SOC1 and AGL24 induce *TFL1* (Fig. 2a-i) and Chromatin Immuno-Precipitation showed that these two TFs bind to the *TFL1* regions that regulate its expression in the SAM (*20*) (Fig. 2j-l). These regions were sufficient to activate a *TFL1* reporter construct by SOC1 and AGL24 in a transient assay (Fig. 2m-n) confirming that both MADS-box TFs are direct regulators of *TFL1*. Since XAANTAL2 (XAL2), a homolog of SOC1 and AGL24 also bound to and induced *TFL1* (*21*), we aggregated the activities of SOC1, AGL24 and XAL2 into a SAX proxy acting as *TFL1* positive regulator (Fig. 3a).

We thus created the SALT network (for SAX, AP1/CAL, LFY, and TFL1; Fig. 3a) made of these 4 regulator sets, auxin (*22*), and F, a flower inducing signal (a proxy for the FT florigen) that increases when the plant ages or is exposed to flower-inducing environmental conditions (*23*, *24*). We also added a short-lived transient early Repressor of *TFL1* (eREP), as a proxy for *TFL1* early repression in the young flower bud performed by the redundant activities of SOC1, AGL24, SHORT VEGETATIVE PHASE, and SEPALLATA4 (*25*).

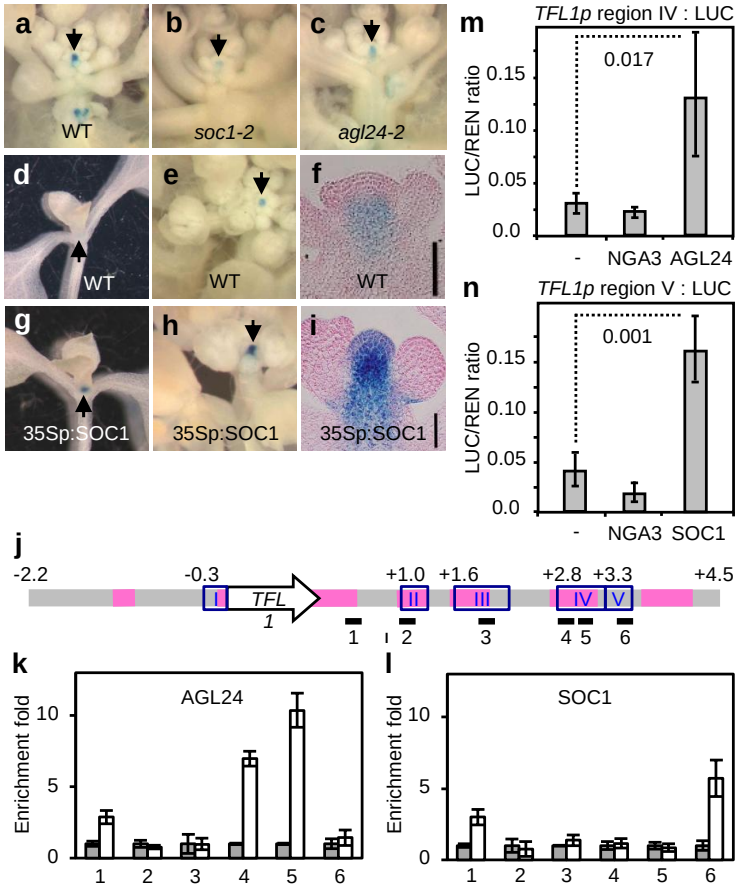

Fig. 2: AGL24 and SOC1 are direct positive regulators of *TFL1*.

(a-c), TFL1p:GUS activity in WT (a), *soc1-2* (b) and *agl24-2* (c) inflorescence apices. (d-i), TFL1p:GUS activity (blue signal) in WT (d-f) and *35Sp:SOC1* (g-i) apices at vegetative (d,g) and flowering (e,f,h,i) stages. (f-i), longitudinal sections through flowering shoots. Arrows mark the SAM. Scale bars in (f) and (i), 40 µm. (j-l) Structure of *TFL1* locus, with regions conserved in Brassicaceae (pink lines), regulatory regions (*20*) (blue boxes I-V), and fragments used in ChIP (black lines 1-6). ChIP experiments on plants expressing a tagged version of AGL24 (k,

white bars) or the WT SOC1 protein (l, white bars) or on control plants (grey bars, see Material and Methods), show that AGL24 binds region IV (k, fragments 4-5) and SOC1 region V (l, fragment 6). A representative biological replicate is shown with the mean =/- SE for three technical replicates. (m,n) Transient assays showing transactivation of the LUCIFERASE (LUC) reporter driven by region IV (activation by 35Sp:AGL24) and region V (activation by 35Sp:SOC1). NGA3 is an unrelated TF used as negative control. Bars denote the mean and standard deviation of three independent biological replicates. *P* values are for the equality of means (Student's t-test).

The steady states of the SALT network correspond to the gene expression patterns observed in wild-type vegetative (low SALT values), inflorescence (high TFL1/SAX, low AP1/CAL/LFY) and flower (low TFL1/SAX, high AP1/CAL/LFY) meristems (Fig. 3b,c, Fig. S2). Above an F threshold value, the network generates a flower or an inflorescence state depending on F and auxin values. Simulations of *tfl1, lfy, ap1 cal* mutants produce expected outputs consistent with experimentally reported gene expressions (*6, 16, 26, 27*) (Fig. 3b, c). The simulated *sax* mutant did not reach a floral state, consistent with the late flowering behavior of the *soc1 agl24* double mutant (*28*).

The modelled gene expression dynamics (Fig. 3d) illuminate the fundamental differences between WT and cauliflower meristems: in a WT flower primordium, F induces *SAX*. SAX and auxin induce *LFY*, that, together with F, induce *AP1/CAL*. AP1 positively feeds back on *LFY* and represses *SAX* (Fig. 3d). *TFL1* expression, that could be induced by SAX and LFY in early floral stages, is constantly repressed, first by eREP and later by SAX plus AP1/CAL. High AP1/CAL and LFY with low TFL1 and SAX expression stabilize the floral fate. In contrast, in the *ap1 cal* flower primordia, the absence of AP1/CAL activity has two consequences: i) *LFY* expression is upregulated only transiently since AP1/CAL positive feedback is missing (Fig. 3d) and ii) *SAX* genes are not repressed by AP1 and thus induce *TFL1* in nascent flower meristems. TFL1 represses *LFY* even further and the meristem returns to a shoot meristem state (Fig. 3d). Note that, the early LFY induction would likely be reinforced (while remaining transient) by incorporating the recently discovered direct induction of LFY by the F partner protein FD (*29*). The SALT model predicts that *SAX* expression should extend over the entire cauliflower. We

analyzed a SOC1-GFP reporter line and indeed observed expansion of its expression domain in *ap1 cal* as compared to WT (Fig. 3e, f).

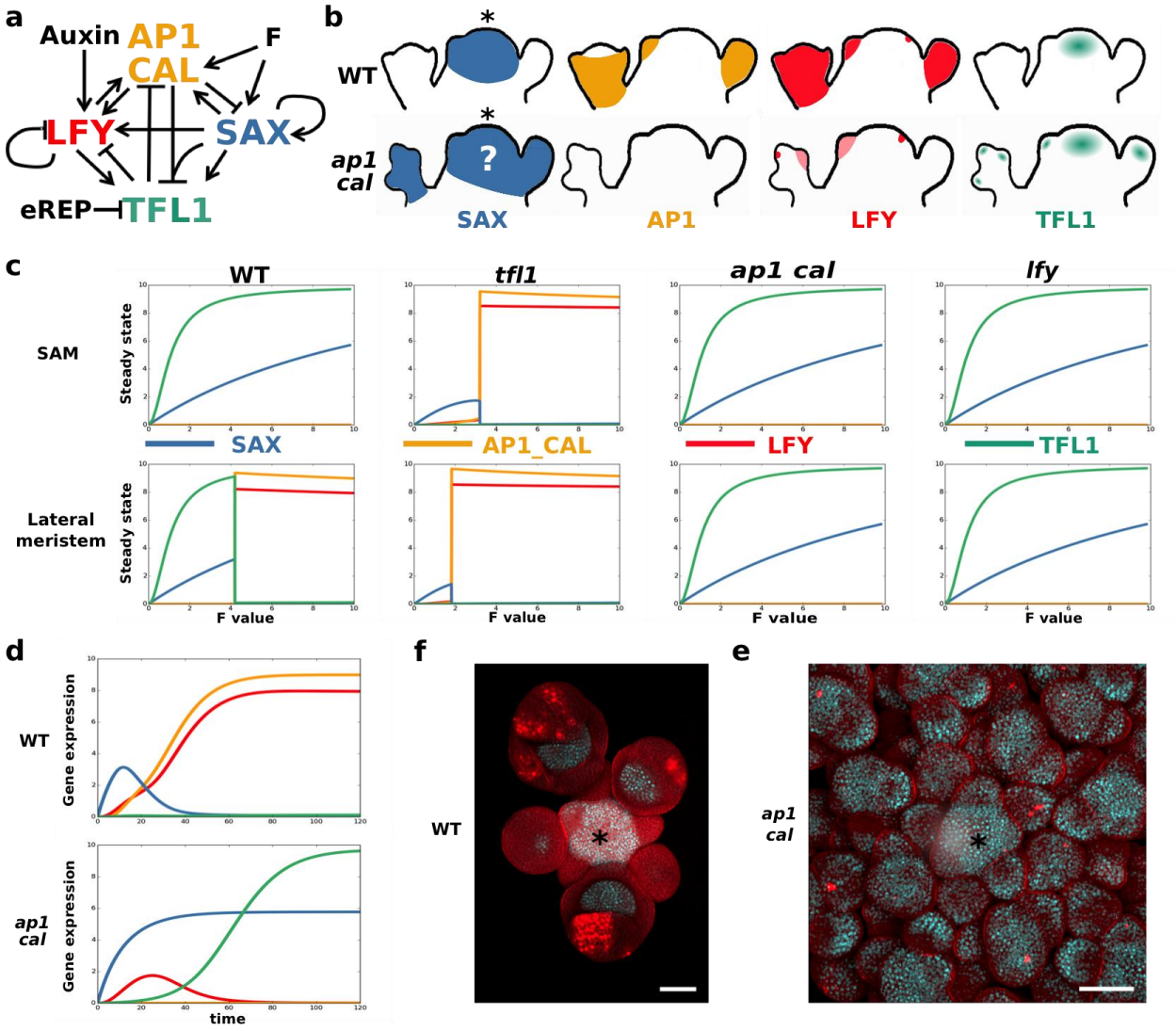

Fig. 3: SALT Gene Regulatory Network model and experimental validation.

(a) SALT GRN network structure (b) Known expression patterns of *SAX*, *AP1/CAL*, *LFY*, and *TFL1* in the SAM and lateral primordia of WT and *ap1 cal* mutant. The question mark indicates a predicted expression pattern of the model. (c) WT, *tfl1*, *ap1 cal* and *lfy* steady states of the model at different F values in the SAM (low auxin) and in lateral meristems (high auxin). The genetic identity predicted for WT and all mutant meristems correspond to the experimentally observed phenotypes. (d) Temporal simulation of gene expression in lateral primordia with high

F value. (e, f) Expression of the SOC1:GFP (white/light blue signal) reporter construct in WT (e) and in the *ap1-7 cal-1* mutant (f) inflorescences. Asterisks mark the SAM. Bar = 50 µm.

The SALT network thus recapitulates realistic gene expressions driving meristem fates. However, a plant architecture does not only depend on meristem fates but also on morphodynamic parameters including molecular thresholds for fate decisions, organ growth rate, delay for meristems to start organ production and organ production rate which are independently regulated. Plant inflorescence architecture thus emerges from the complex interaction between the floral GRN and morphodynamic parameters. This is illustrated here by the *lfy* and *ap1 cal* mutants that have the same GRN outputs (Fig. 3c) but markedly different architectures (*6*, *27*). To study how this interaction operates in Arabidopsis, we integrated the SALT GRN in a 3D plant computational model implemented as an L-system (see Supplementary materials Modeling Methods).

A multi-scale model generates Arabidopsis cauliflower structures

The 3D model is made of the 4 types of organs that shape plant above-ground architecture: meristems, internodes, leaves and flowers (Fig. 4a, Supplementary materials). Each meristem's identity (vegetative, inflorescence and floral) is determined by the GRN steady state, computed at each time step as a function of the meristem's previous state and external factors (auxin and F). The GRN model is implemented as single compartment ordinary differential equations (Supplementary materials Modeling Methods). We assume that the GRN dynamics is faster than growth and reaches its steady state within a time step. A set of growth rules defines meristem production: a vegetative meristem produces a compressed stem (non-elongated internodes) with rosette leaves; an inflorescence meristem produces an elongating internode, a cauline leaf and a new shoot meristem in the leaf axil; a floral meristem produces an internode terminating with a flower meristem, devoid of bracts (leaf-like organs subtending flowers) since they are repressed by LFY (*6*)). Each newly generated axillary meristem begins with maximal auxin level (*22*), SAX/LFY/AP1/CAL values inherited from the parent meristem, together with a fraction of the parent TFL1 value as, in the real plant, this non-cell autonomous protein is present in the primordia region (*30*). To match the wild-type plant architecture, indeterminate meristems at orders >2 (Fig. 4a) were kept quiescent, a likely effect of apical dominance (the inhibition of

lateral meristem outgrowth) (Fig. S3a). The model also contains rules describing organ growth dynamics (internode and leaf elongation, flower growth, organ production rate, growth initiation delay). Simulated plants start with a single vegetative SAM and repeatedly produce new organs according to the GRN, the morphodynamic rules and an input value of F.

By adjusting the GRN and morphodynamic parameters within a range of plausible values (Supplementary materials), we successfully calibrated the model to produce realistic architectures for wild-type and *lfy* plants (Supplementary Movies 1-2), as well as for the *tfl1* mutant (Fig. 4b-d) and a non-flowering phenotype for the *sax* mutant. However, our simulations could not generate a realistic *ap1 cal* mutant growing without bract/cauline leaves and displaying high order meristems (Fig. S3a-b) suggesting that the cauliflower phenotype involves additional regulations. We reasoned that laterally produced *ap1 cal* inflorescence meristems are different from those produced in other genotypes as, according to our GRN, they have been transiently exposed to LFY expression (Fig. 3d). Several pieces of evidence suggest that this transient LFY expression, already known to repress bracts (*6*), could also contribute to high-order meristem release. First, the outgrowth of otherwise inhibited axillary meristems in the rosette is stimulated by ectopic expression of LFY (or a LFY allele) (*31*, *32*). Second, it was established that the *lfy ap1 cal* triple mutant does not form cauliflowers (*6*) and we found that, in this mutant, the number of high-order meristems is significantly reduced as compared to *ap1 cal* (Fig. S3d-h), thus supporting our hypothesis.

We abstracted this critical molecular pathway, by introducing in the model a factor X upregulated when LFY exceeds a minimal threshold level. Upregulated factor X releases high-order meristem growth and suppresses the bract. This was sufficient to unlock the recursive growth of lateral meristems and to generate the *ap1 cal* curd structure that arises from the transient but irreversible exposure of meristems to the floral signal without any alteration of wild type growth dynamics (Fig. 4e,h, Supplementary Movie 3). Overall, our work shows that the *ap1 cal* and *lfy* architectures are different (Fig. 3c) because the molecular histories of their inflorescence meristems are different, thereby revealing the existence of a developmental hysteresis.

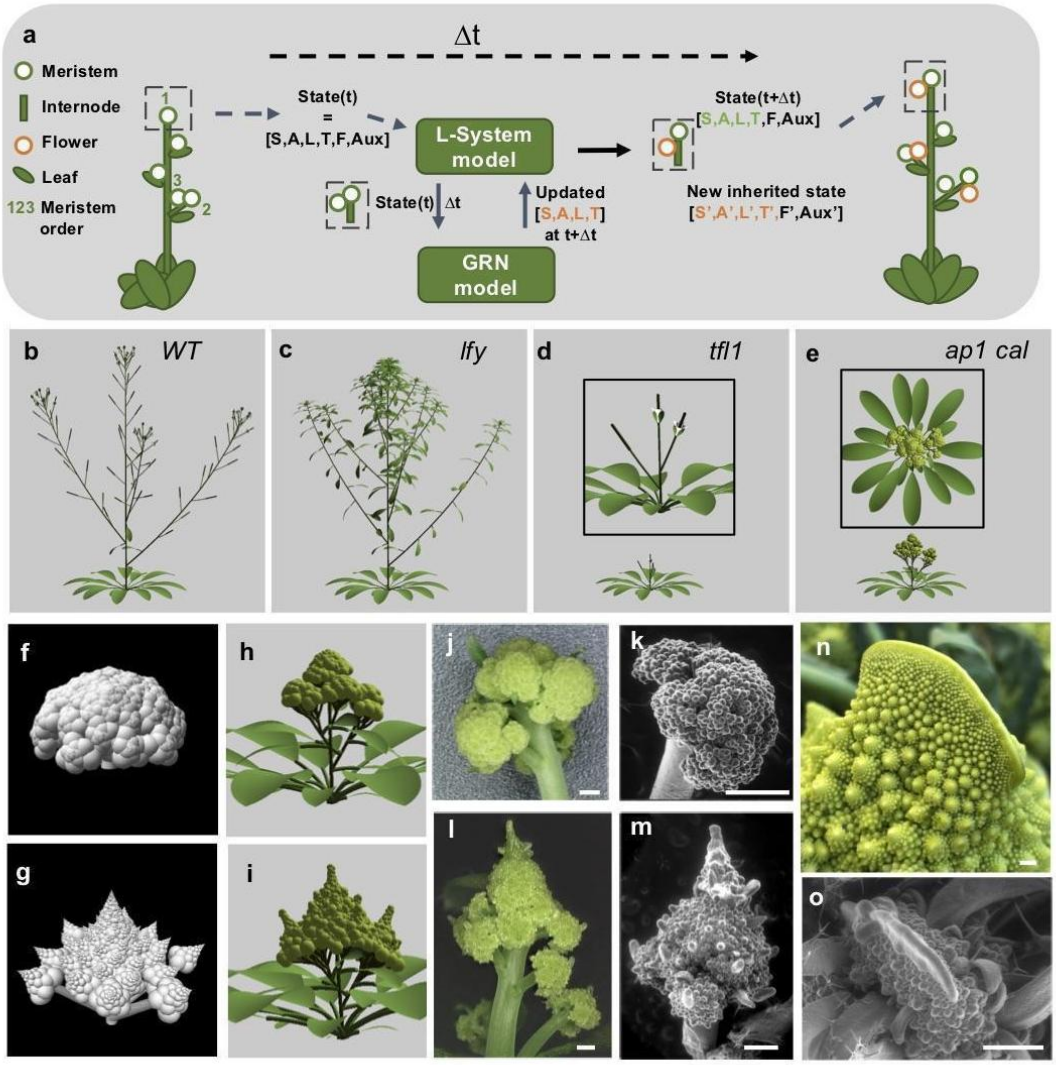

234

235 **Fig. 4: Simulation and assessment of a GRN-based plant development model.**
236 (a) Schematic representation of the multi-scale model of Arabidopsis development. Each
237 meristem state is composed of signal levels (auxin, F) and a GRN steady state. At time *t*, the
238 plant is made up of a collection of organs (left). At time $t+\Delta t$ (right) the model updates the signal
239 levels and GRN state in each meristem. The steady state defines the identity of the meristems
240 (vegetative, inflorescence or flower) used to compute meristem lateral productions. Green
241 numbers indicate meristem order (b-e). Plant morphologies obtained in the WT (b), *lfy* (c), *tfl1*
242 (d) and *ap1 cal* (e) simulations. Simulated morphologies with constant (f,h) or increased
243 meristem size (g,i) in a simplified (f,g) and the Arabidopsis model (h,i). Light micrographs (j,l,n)
244 and s.e.m (k,m,o) of cauliflower structures in Arabidopsis *ap1 cal* (j, k), Arabidopsis *ap1 cal*

clv3 (l, m, o) and Romanesco (n). Uninduced *AP1:GR* transgene is present in plants j-m. Scale bars = 500 µm.

Growth dynamics define cauliflower and Romanesco curd structures

Our work in Arabidopsis offers a conceptual framework to explain how inflorescence architecture emerges from coupling a floral GRN to morphodynamic parameters. We wondered whether modifications affecting components of this framework could also explain the architecture of the cauliflowers that arose during domestication, namely the edible *Brassica oleracea (Bo)* var. *botrytis (Bob)* and its Romanesco variant. Whether similar genetic defects as in Arabidopsis are responsible for curd development in *B. oleracea* is still debated (*4*, *5*). To further investigate this point, we analysed RNA-seq data of *Bob* curds: we confirmed the previously identified mutation in the *BobCAL* gene (Fig. S4a)(*4*, *5*, *7*) and observed that the two *AP1* paralogs (*BobAP1-a* and *BobAP1-c)* are expressed at much lower levels than in cabbage (*Bo* var. *capitata)* inflorescences (Fig. S4b). These functional proteins are induced with a delay only when the cauliflower elongates and start forming normal flowers (*3*, *33*). Comparing cauliflower and cabbage sequences, we identified differences in binding sites for candidate regulators of *BoAP1* that could account for their delayed activation (Fig. S4d). The combination of BoCAL inactivation and *BobAP1-a/c* expression delay (heterochrony due to *cis* or *trans* mutations) thus likely participates to *Bob* curd development. Similar to Arabidopsis *ap1 cal*, cauliflowers have meristems of higher maximal order ($n \geq 7$) than cabbages (n = 3-4) (Fig. S5). Nevertheless, the development of single massive cauliflower curds is not the exact equivalent of the Arabidopsis mutant (*3*, *5*) and involves additional multifactorial alterations of morphodynamics parameters (such as reduction of internode elongation and branches diameter increase).

The conical shapes appearing in Romanesco spirals at all scales (Fig. 1f) represent an additional geometric variation obtained through domestication that seems to be associated with a change in morphodynamic parameters. Indeed, several such parameters remain constant during cauliflower development but vary in Romanesco (*34*): i) the plastochron, the time between two successive meristem productions, ii) the number of visual spirals originating from a given meristem, iii) the time (measured in number of plastochrons) needed before a lateral primordium starts producing its own primordia (or lateral production onset delay), and iv) the size of the meristems. Whether

some of these parameters are causal to the Romanesco phenotype remains unclear but phyllotaxis studies (*1*, *35*, *36*) indicate that the first three parameters are linked to the meristem size: an augmentation of the size of the meristem central zone should decrease the plastochron, which in turn increases the number of spirals, and the lateral production onset delay. We thus hypothesized that passing from a constant to a decreasing plastochron in meristems could change cauliflower into Romanesco morphologies. We first tested this *in silico* using a simplified, purely geometric model of curd growth, independent from the Arabidopsis GRN and specific growth dynamics (Supplementary materials). A decreasing plastochron was sufficient to produce Romanesco shapes (Fig. 4g) whereas constant values of this parameter produce cauliflower morphologies (Fig. 4f).

We then introduced the same change in the more complex GRN-based, Arabidopsis cauliflower architectural model, while keeping its organ growth dynamics as calibrated on the WT. Although not as complete as in the purely geometric model, the curd changed towards a "Romanesco-like" morphology with typical conical curd shapes (Fig. 4h, i). We then tested this hypothesis experimentally in Arabidopsis by altering the size of the meristem directly. We achieved this by introducing a mutation in the *CLAVATA3* (*CLV3*) gene that controls meristem homeostasis and induces an increase of the meristem central zone during growth (*37*, *38*). As predicted by our analysis, introduction of a *clv3* mutation in *ap1 cal* Arabidopsis mutant modified the curd shape, which lost its round morphology and acquired a more conical shape, with similar structures at different scales, features recognized as hallmarks of Romanesco curds (*39*) (Fig. 4l-m). Two additional pieces of evidence support the hypothesis that meristem homeostasis is perturbed in Romanesco curds: they occasionally show fasciation, a feature typical of meristem enlargement also observed in *clv3* or *ap1 cal clv3* mutants (Fig. 4n,o)(*37*). Moreover, the expression of *CLV3* (and possibly two other genes acting in the same pathway)(*38*) are lower in Romanesco curds than in cauliflowers (Fig. S6). Altogether, these observations establish that meristem size regulates the final curd morphology through control of plastochron value.

These results reveal how fractal patterns can be generated through growth and developmental networks that alter identities and meristem dynamics. Our data, GRN and growth models now clarify the molecular and morphological changes over time by which meristems gain different

identities to form the highly diverse and fascinating array of plant architectures found throughout nature and crops.

References and Notes:

1. C. Godin, C. Golé, S. Douady, *Development*. **147**, dev165878 (2020).

2. C. F. Quiros, M. W. Farnham, in *Genetics and Genomics of the Brassicaceae*, R. Schmidt, I. Bancroft, Eds. (Springer New York, 2011), pp. 261–289.

3. D. V. Duclos, T. Björkman, *J. Exp. Bot*. **59**, 421–433 (2008).

4. L. B. Smith, G. J. King, *Mol. Breeding*. **6**, 603–613 (2000).

5. N. Guo, S. Wang, L. Gao, Y. Liu, X. Wang, E. Lai, M. Duan, G. Wang, J. Li, M. Yang, M. Zong, *BMC Biology*. **19**, 93 (2021).

6. J. L. Bowman, J. Alvarez, D. Weigel, E. M. Meyerowitz, D. R. Smyth, *Development*. **119**, 721 (1993).

7. S. Kempin, B. Savidge, M. Yanofsky, *Science*. **267**, 522 (1995).

8. G. Denay, H. Chahtane, G. Tichtinsky, F. Parcy, *Curr. Opin. Plant Biol*. **35**, 15–22 (2017).

9. A. Pajoro , S. Biewers, E. Dougali, F. Leal Valentim, M. A. Mendes ,A. Porri, G. Coupland, Y. Van de Peer, A.D. Van Dijk, L. Colombo, B. Davies, *J. Exp. Bot*. **65**, 4731–4745 (2014).

10. B. Thomson, F. Wellmer, *Curr. Top. Dev. Biol*. **131**, 185–210 (2019).

11. K. E. Jaeger, N. Pullen, S. Lamzin, R. J. Morris, P. A. Wigge, *Plant Cell*. **25**, 820 (2013).

12. C. Espinosa-Soto, P. Padilla-Longoria, E. R. Alvarez-Buylla, *Plant Cell*. **16**, 2923–2939 (2004).

13. F. L.Valentim *et al*, *PLOS ONE*. **10**, e0116973 (2015).

14. P. Prusinkiewicz, Y. Erasmus, B. Lane, L. D. Harder, E. Coen, *Science*. **316**, 1452 (2007).

15. K. Goslin *et al.*, *Plant Physiol.* **174**, 1097 (2017).

16. C. Ferrandiz, Q. Gu, R. Martienssen, M. F. Yanofsky, *Development*. **127**, 725 (2000).

17. D. Bradley, O. Ratcliffe, C. Vincent, R. Carpenter, E. Coen, *Science*. **275**, 80 (1997).

18. X. Hou *et al.*, *Nat. Commun*. **5**, 4601 (2014).

19. S. K. Yoo *et al.*, *Plant Physiol.* **139**, 770 (2005).

20. A. Serrano-Mislata *et al.*, *Development*. **143**, 3315 (2016).

21. R. V. Pérez-Ruiz *et al.*, *Mol. Plant*. **8**, 796–813 (2015).

22. D. Reinhardt *et al.*, *Nature*. **426**, 255–260.

23. P. A. Wigge, *Curr. Biol*. **21**, R374-378 (2011).

24. J. Putterill, E. Varkonyi-Gasic, *Curr. Opin. Plant Biol*. **33**, 77–82 (2016).

25. C. Liu *et al.*, *Dev. Cell*. **24**, 612–622 (2013).

26. O. J. Ratcliffe *et al.*, *Development*. **125**, 1609 (1998).

27. D. Weigel, J. Alvarez, D. R. Smyth, M. F. Yanofsky, E. M. Meyerowitz, *Cell*. **69**, 843–859 (1992).

28. S. D. Michaels *et al.*, *Plant J*. **33**, 867–874 (2003).

29. Y. Zhu *et al.*, *Nat. Commun*. **11**, 5118 (2020).

30. L. Conti, D. Bradley, *Plant Cell*. **19**, 767 (2007).

31. H. Chahtane *et al.*, *Plant J*. **74**, 678–689 (2013).

32. D. Weigel, O. Nilsson, *Nature*. **377**, 495–500 (1995).

33. X. Sun *et al.*, *Environ. Exp. Bot.*. **155**, 742–750 (2018).

34. M. Kieffer, M. P. Fuller, A. J. Jellings, *Planta*. **206**, 34–43 (1998).

35. S. Douady, Y. Couder, *J. Theor. Biol*. **178**, 255–273 (1996).

36. Y. Refahi *et al.*, *eLife*. **5**, e14093 (2016).

37. J. C. Fletcher, *Science*. **283**, 1911–1914 (1999).

38. M. Kitagawa, D. Jackson, *Annu. Rev. Plant Biol.* **70**, 269–291 (2019).

39. L. E. Watts, *Euphytica*. **15**, 111–115 (1966).

40. A. Maizel, D. Weigel, *Plant J*. **38**, 164–171 (2004).

41. V. Grandi, V. Gregis, M. M. Kater, *Plant J*. **69**, 881–893 (2012).

42. R. G. H. Immink *et al.*, *Plant Physiol.* **160**, 433 (2012).

43. I. Kardailsky, *Science*. **286**, 1962–1965 (1999).

44. H. Lee, *Genes Dev*. **14**, 2366–2376 (2000).

45. V. Gregis, A. Sessa, C. Dorca-Fornell, M. M. Kater, *Plant J.* **60**, 626–637 (2009).

46. H. Onouchi, M. I. Igeño, C. Périlleux, K. Graves, G. Coupland, *Plant Cell*. **12**, 885–900 (2000).

47. M. Koornneef, C. J. Hanhart, J. H. van der Veen, *Mol. Gen. Genet.* **229**, 57–66 (1991).

48. F. Wellmer, M. Alves-Ferreira, A. Dubois, J. L. Riechmann, E. M. Meyerowitz, *PLoS Genet*. **2**, e117 (2006).

49. R. A. Jefferson, T. A. Kavanagh, M. W. Bevan, *EMBO J.* **6**, 3901–3907 (1987).

50. N. Bechtold, J. Ellis, G. Pelletier, *C. R. Acad. Sci. Paris, Life Sci*. **316**, 1194–1199 (1993).

51. N. Bechtold, D. Bouchez, in *Gene Transfer to Plants*, I. Potrykus, G. Spangenberg, Eds. (Springer Berlin Heidelberg, 1995) pp. 19–23.

52. M. Trigueros *et al.*, *Plant Cell*. **21**, 1394–1409 (2009).

53. I. Mitsuhara *et al.*, *Plant Cell Physiol*. **37**, 49–59 (1996).

54. R. Hellens *et al.*, *Plant Methods*. **1**, 13 (2005).

55. Z. Feng *et al.*, *Cell Res*. **23**, 1229–1232 (2013).

56. W. Yan, D. Chen, K. Kaufmann, *Plant Methods*. **12**, 23 (2016).

57. S. Bensmihen *et al.*, *FEBS Lett*. **561**, 127–131 (2004).

58. S. J. Clough, A. F. Bent, *Plant J.* **16**, 735–743 (1998).

59. N. Prunet, K. Duncan, *J. Exp. Bot*. **71**, 2898–2909 (2020).

60. A. Sessions, D. Weigel, M. F. Yanofsky, *Plant J.* **20**, 259–263 (1999).

61. D. Weigel, J. Glazebrook, *Arabidopsis: a laboratory manual* (Cold Spring Harbor Laboratory Press, New York, 2002).

62. C. Dorca-Fornell *et al.*, *Plant J*. **67**, 1006–1017 (2011).

63. C. Belser *et al.*, *Nat. Plants*. **4**, 879–887 (2018).

64. J. Yu *et al.*, *BMC Genomics*. **15**, 3 (2014).

65. H. Lv *et al.*, *Sci Rep*. **10**, 12394 (2020).

66. O. Fornes *et al.*, *Nucleic Acids Res*. **48**, D87-D92 (2019).

67. E. Moyroud *et al.*, *Plant Cell*. **23**, 1293 (2011).

68. B. H. Toyama, M. W. Hetzer, *Nat. Rev. Mol. Cell Bio*. **14**, 55–61 (2013).

69. A. Jolma *et al.*, *Nature*. **527**, 384–388 (2015).

70. S. Legewie, H. Herzel, H. V. Westerhoff, N. Blüthgen, *Mol. Syst. Biol*. **4**, 190 (2008).

71. S. Belikov, O. G. Berg, Ö. Wrange, *Nucleic Acids Res*. **44**, 3045–3058 (2015).

72. S. Mangan, U. Alon, *Proc. Natl. Acad. Sci. U.S.A.* **100**, 11980–11985 (2003).

73. P. Prusinkiewicz, A. Lindenmayer, *The algorithmic beauty of plants* (Springer-Verlag, New York, 1990).

74. F. Boudon, C. Pradal, T. Cokelaer, P. Prusinkiewicz, C. Godin, *Front. Plant Sci.* **3** (2012).

75. L. Mündermann, Y. Erasmus, B. Lane, E. Coen, P. Prusinkiewicz, *Plant Physiol.* **139**, 960–968 (2005).

76. C. M. Winter *et al.*, *Dev. Cell*. **20**, 430–443 (2011).

77. D. A. William *et al.*, *Proc. Natl. Acad. Sci. U.S.A.* **101**, 1775 (2004).

78. R. Benlloch *et al.*, *Plant J*. **67**, 1094–1102 (2011).

79. D. Wagner, R. W. M. Sablowski, E. M. Meyerowitz, *Science*. **285**, 582 (1999).

80. F. Parcy, O. Nilsson, M. A. Busch, I. Lee, D. Weigel, *Nature*. **395**, 561 (1998).

81. S. Hanano, K. Goto, *Plant Cell*. **23**, 3172 (2011).

82. O. J. Ratcliffe, D. J. Bradley, E. S. Coen, *Development*. **126**, 1109 (1999).

83. D. Goretti *et al.*, *Plant Physiol.*, **182** 2081-2095 (2020).

84. J.-H. Jung, H.-J. Lee, J. Y. Ryu, C.-M. Park, *Mol. Plant*. **9**, 1647–1659 (2016).

85. P. A. Wigge *et al.*, *Science*. **309**, 1056 (2005).

86. S. Collani, M. Neumann, L. Yant, M. Schmid, *Plant Physiol.* **180**, 367–380 (2019).

87. M. Abe, *Science*. **309**, 1052–1056 (2005).

88. P. Teper-Bamnolker, A. Samach, *Plant Cell*. **17**, 2661–2675 (2005).

89. M. Romera-Branchat *et al.*, *Cell Rep*. **31**, 107717 (2020).

90. S.J. Liljegren, C. Gustafson-Brown, A. Pinyopich, G. S. Ditta, M. F. Yanofsky, *Plant Cell*. **11**, 1007 (1999).

91. K. Kaufmann *et al.*, *Science*. **328**, 85 (2010).

92. J. Lee, M. Oh, H. Park, I. Lee, *Plant J*. **55**, 832–843 (2008).

93. J. Moon, H. Lee, M. Kim, I. Lee, *Plant Cell Physiol*. **46**, 292–299 (2005).

94. C. Liu *et al.*, *Development*. **135**, 1481 (2008).

95. N. Yamaguchi *et al.*, *Dev Cell*. **24**, 271–282 (2013).

96. W. Li *et al.*, *Sci. Signal.* **6**, ra23 (2013).

97. O. Nilsson, I. Lee, M. A. Blázquez, D. Weigel, *Genetics*. **150**, 403–410 (1998).

98. A. Serrano-Mislata *et al.*, *Plant Signal. Behav*. **12**, e1370164 (2017).

99. C. Liu *et al.*, *Development*. **134**, 1901 (2007).

100. H. Yu, T. Ito, F. Wellmer, E. M. Meyerowitz, *Nat. Genet*. **36**, 157 (2004).

101. Z. Tao *et al.*, *Plant J*. **70**, 549–561 (2012).

102. H. Yu, Y. Xu, E. L. Tan, P. P. Kumar, *Proc. Natl. Acad. Sci. U.S.A.* **99**, 16336–16341 (2002).

103. J.-W. Wang, B. Czech, D. Weigel, *Cell*. **138**, 738–749 (2009).

104. S. D. Michaels, E. Himelblau, S. Y. Kim, F. M. Schomburg, R. M. Amasino, *Plant Physiol.* **137**, 149–156 (2005).

105. I. Searle, *Gene. Dev*. **20**, 898–912 (2006).

106. R. Borner *et al.*, *Plant J*. **24**, 591–599 (2000).

107. A. Samach, *Science*. **288**, 1613–1616 (2000).

108. S. R. Hepworth, *The EMBO J*. **21**, 4327–4337 (2002).

Acknowledgments

We thank Anne-Marie Chèvre, Richard Immink, Rüdiger Simon, Lars Ostergaard and Mariana Benitez for advice, Teva Vernoux, Chloe Zubieta and Hicham Chahtane for proofreading and useful feedback on the manuscript, Dominique Tardy, Eric Giraud, Renaud Dumas and Vincent Martin (OBS, France) for providing cauliflower samples and Lydia Bousset Vaslin for images and branch counting, Frédéric Boudon for help with L-Py, Richard Immink (Wageningen, Netherlands), C. Ferrándiz (IBMCP; Spain), George Coupland (MPIPZ, Germany), Miguel

Ángel Blázquez (IBMCP, Spain), Richard Amasino (UWM, USA) and the European Arabidopsis Stock Centre for providing seeds, Vincent Berger (CEA/DRF) for the Keyence microscope, Christine Lancelon-Pin (Plateau de microscopie électronique - ICMG. CERMAV-CNRS) for SEM experiments.

Funding

This project received support from the INRAE Caulimodel project (FP and CG), Inria Project Lab Morphogenetics (CG, EA and FP), the ANR BBSRC Flower model project (FP and CG), the GRAL LabEX (ANR-10-LABX-49-01) with the frame of the CBH-EUR-GS (ANR-17-EURE-0003), EU H2020 773875 ROMI project funding (CG), the Spanish Ministerio de Ciencia Innovación and FEDER (grant no. PGC2018-099232-B-I00)(FM).

Author contributions

ChG and FP conceived the study

ChG, EA, EF performed the modelling

ASM, CaG, DB, FM, FP, GT, MK, MLM, VG designed and performed the plant experiments

NP performed the confocal imaging experiment

JL analysed the RNA-seq and genomic data

ChG, FP and EA wrote the paper with the help of all authors

Competing interests

The authors declare no competing interests.

Data and Materials Availability

All data are in the main paper or the supplement.

All plant materials are available upon request.

The following secure token has been created to allow review of record GSE150627 while it remains in private status: khkjgckmdtkhpgb.

All source codes to run the simulations are available as supplementary archive file (description of installation and execution available as README.txt.

476
477
478 **Supplementary Materials:**
479 Materials and Methods
480 Figures S1 to S6
481 Tables S1 toS3
482 Movies S1 to S3
483 Code archive file: Architecture-model.zip
484 References (41-108)
485 MDAR Reproducibility Checklist
486
487
488